OPEN ACCESS
PAPER

Mongolian Journal of Geography and Geoecology - MJGG

Received: 12 May 2025; Accepted: 04 July 2025; Published online: 1 September 2025
https://doi.org/10.5564/mjgg.v62i46.4138

Seasonal water yield modelling of the Baidrag River basin

***Corresponding author**
Purevsuren Munkhtur
purevsurenm@mas.ac.mn

CITATION
Purevsuren M, Batnyam Ts, Bayanjargal B, Odbaatar E (2025) Seasonal Water Yield Modelling of The Baidrag River Basin. *Mongolian Journal of Geograhy and Geoecology,* 62(46), 1–11.
https://doi.org/10.5564/mjgg.v62i46.4138

Purevsuren Munkhtur[1,*], Batnyam Tseveengerel[1], Bayanjargal Bumtsend[1], Odbaatar Enkhjargal[1]

[1]*Institute of Geography and Geoecology, Mongolian Academy of Sciences, Ulaanbaatar 15170, Mongolia*

ABSTRACT

Water yield plays a critical role in sustaining ecological balance and supporting ecosystem services, yet it exhibits significant spatial and seasonal variability. Estimating water yield in data-scarce regions remains challenging, emphasizing the importance of model-based approaches. This study evaluated the performance of the Integrated Valuation of Ecosystem Services and Tradeoffs - Seasonal Water Yield Model (InVEST-SWYM) for simulating seasonal water yield in the Baidrag River Basin, Mongolia, over the period 2000–2020. The model was applied using key input parameters, including monthly precipitation, evapotranspiration, a digital elevation model, land use and land cover data, and soil characteristics derived from satellite imagery and primary sources. Key outputs included monthly and annual quickflow (QF), baseflow (B), and actual evapotranspiration (AET). Results revealed increasing trends in precipitation (180.9–253.7 mm/year) and quickflow (15.15-21.77 mm/year), with peak runoff in July. AET increased from 163.4 mm to 230.14 mm, while potential evapotranspiration (PET) declined from 1314.9 mm to 1139.6 mm. Baseflow remained low (0.1–4 mm), with higher values in northern and north-eastern zones. Quickflow showed strong seasonality and was spatially concentrated in the northern and western sub-basins. These patterns were interpreted to reflect the combined influence of precipitation distribution, topographic gradients, and land cover characteristics, based on visual analysis of spatial model outputs. The results highlight reduced flows during winter due to frozen ground and elevated summer flows linked to precipitation peaks. The seasonal quickflow estimation was validated by comparing the predicted results with observed streamflow data from the Baidrag-Baidrag gauging station for the years 2000 and 2020. To assess statistical correlation and reliability, Nash–Sutcliffe Efficiency (NSE) and Percent Bias (PBIAS) were calculated. NSE values were 0.77 and 0.79 for 2000 and 2020, respectively, with PBIAS values of 25.64 and –23.64. The model tended to overestimate streamflow during spring snowmelt (May) and underestimate it during the summer rainfall season, likely due to bias in CHIRPS precipitation data.

KEYWORDS

Quickflow, Baseflow, Evapotranspiration, Ecosystem service, InVEST-SWY model

1. INTRODUCTION

Water yield is a vital ecosystem service that supports forestry, aquaculture, and energy production while contributing to the ecological balance [1]. As a key component of natural ecosystems, the valuation of water yield has become an essential tool for informing policy decisions and guiding conservation efforts. [2]. Despite its significance, the term "water yield" is often used interchangeably with "watershed yield", referring either to the long-term average runoff or the total runoff volume within a specific period [3]. It generally represents the total runoff in a given region [4] and can be estimated at annual, monthly, or daily. Monitoring seasonal water yield (SWY) is particularly important [5] due to its substantial influence on industrial, agricultural, and domestic activities [6], [7].

Hydrological modeling, however, remains complex due to the interplay of multiple interdependent factors, such as climatic conditions, soil characteristics, land cover types, and topography, which all exhibit spatial and temporal variability [8]. Advances in geographic information systems (GIS) have facilitated the development of hydrological models that account for these complexities. Several studies have employed models like SWAT, RRI, HBV, and HEC-HMS models to estimate both annual and seasonal water yield. In Mongolia, research has focused on calibrating hydrological models to analyze eco-hydrological processes [9], land cover changes [10], and the effects of climate change on flow variation [11]. However, these studies have been limited by the use of a narrow range of models and locations, highlighting the need for further research to expand water yield modeling in the region.

This study has three main objectives: (1) to test the applicability of the InVEST Seasonal Water Yield Model (InVEST-SWYM) in the Baidrag River Basin, a data-scarce, semi-arid region of Mongolia, (2) to use the model outputs to explore spatial and temporal patterns of water yield components, particularly seasonal patterns of quickflow from 2000 and 2020, and (3) to validate the model results with observed data. The InVEST-SWYM was selected due to its advantages, including minimal input parameter requirements, low input dependency, and broad applicability [12]. Unlike the InVEST annual water yield model, which estimates total annual yield based on precipitation and evapotranspiration, the seasonal model distinguishes between quickflow and baseflow, offering a more detailed representation of hydrological processes at the pixel level. By providing spatially explicit raster-based outputs, InVEST-SWYM enables a comprehensive analysis of water yield variations while contributing to hydrological research in Mongolia and informing water resource management in data-limited regions.

2. RESEARCH METHOD

2.1. Study area

The Baidrag River Basin, located in central Mongolia, is a key hydrological system influenced by diverse topographical and climatic conditions. It is bounded by the Khangai Mountains Drainage Basin to the north, the Gobi Altai Mountains Drainage Basin to the south, Khyargas Lake and the Zavkhan River to the west, and Orog Lake and the Tuin River to the east [13]. The basin covers an area of approximately 1,820,900 hectares, encompassing the territories of nine soums in Bayankhongor Province (Figure 1). The Baidrag River originates from the confluence of three primary tributaries: the Zuun, Dund, and Baruun Rivers. These tributaries flow from the Khan Jargalant Mountain range of the Khangai Mountains, with headwaters originating at Khuungiin Ereen Mountain (3,120 m) and Suviin Shombon Mountain (3,380 m) [14]. Downstream, additional tributaries such as the Zag and Tsagaan Turuut Rivers contribute to the flow before the Baidrag River ultimately discharges into Buuntsagaan Lake.

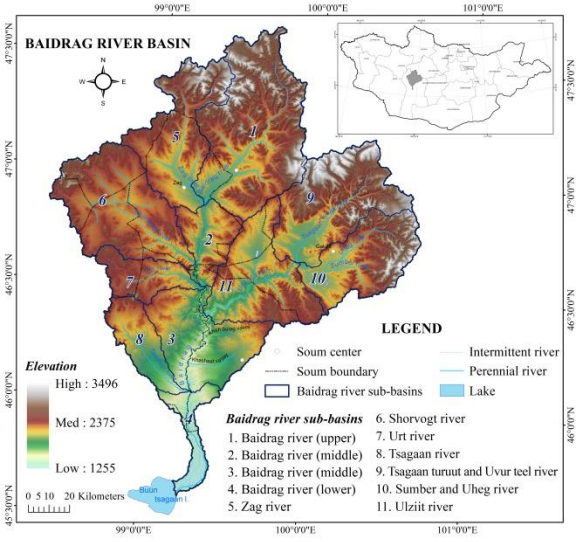

Figure 1. Study area map

Located at the Khangai Mountain foothills, the basin experiences distinct climatic patterns—zonal in the south, gradually weakening at higher elevations due to the influence of mountainous terrain. The mean annual air temperature varies between 3°C and -7°C, with seasonal fluctuations ranging from -14°C to -24°C in winter and 8°C to 10°C in summer [13].

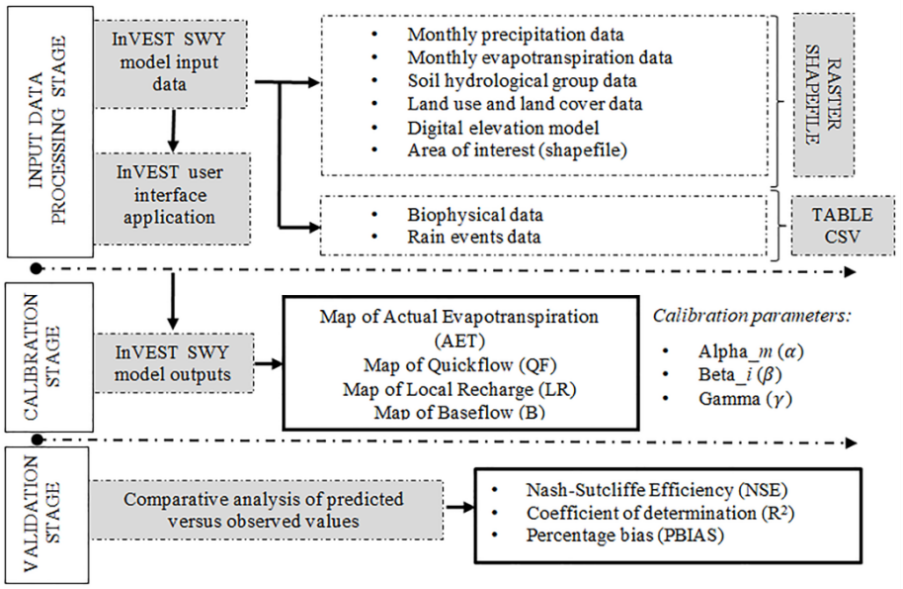

Figure 2. Schematic diagram of the study method

2.2. InVEST Seasonal Water Yield model

The InVEST-SWYM model is a hydrological model designed to estimate the spatial distribution of quickflow and baseflow within a watershed, providing monthly runoff estimates essential for water resource management [15]. The model applies the Curve Number (CN) approach to calculate quickflow, while baseflow is estimated using a physically based approach [15]. The primary outputs of InVEST-SWYM include monthly and annual quickflow (QF), baseflow (B), and actual evapotranspiration (AET).

Quickflow represents the portion of precipitation that rapidly runs off the land surface. The model determines QF using the CN method, which accounts for soil and land cover characteristics. High CN values (e.g., clay soils and low vegetation cover) indicate greater runoff potential, whereas low CN values (e.g., sandy soils and dense vegetation cover) indicate lower runoff potential. Quickflow is calculated using an exponential distribution of daily precipitation depths on rainy days:

$$f(p) = \frac{1}{a_{i,m}} \exp\left(-\frac{p}{a_{i,m}}\right) \quad (1)$$

$$a_{i,m} = \frac{P_{i,m}}{n_m}/25.4 \quad (2)$$

Where, $a_{i,m}$ = Mean rain depth on a rainy day at pixel i on month m [inches],
$n_{i,m}$ = Number of rainfall events at pixel i on month m,
$P_{i,m}$ = Monthly precipitation at pixel i in month m [mm],

For non-stream pixels, QF is determined using the following equation:

$$QF_{i,m} = n_m * \left(\left(a_{i,m} - S_i\right) \exp\left(-\frac{0.2S_i}{a_{i,m}}\right) + \frac{S_i^2}{a_{i,m}} \exp\left(\frac{0.8S_i}{a_{i,m}}\right) E_1\left(\frac{S_i}{a_{i,m}}\right)\right) * \left(25.4\left[\frac{mm}{in}\right]\right) \quad (3)$$

$$S_i = \frac{1000}{CN_i} - 10[in] \quad (4)$$

Where, CN_i = Curve number for pixel i,
E_1 = Exponential integral function,
$E_1(x) = \int_1^\infty \frac{e^{-xt}}{t} dt$, and 25.4 is a conversion factor from inches to millimetres.

Baseflow is the component of infiltrated water that percolates through the soil and eventually contributes to streamflow. The InVEST-SWYM estimates baseflow using pixel-wise calculations, with only positive local recharge values contributing to baseflow. Pixels with negative LR values are assigned zero baseflow. The model determines baseflow using:

$B_{sum,j} = L_{sum,j}$ If k is a non-stream pixel or,

$B_{sum,j} = L_{sum,j} \Sigma_{k \in \{cells\ to\ which\ cell\ i\ porus\}} P_{jk}$, If k is a stream pixel
Where,
$L_{sum,j}$ = Cumulative recharge at upstream,
P_{jk} = Flow proportion from cell j to k, and subsequent baseflow is derived straight away from the cumulative baseflow percentage leave-taking cell j, respecting the obtainable recharge to the cumulative recharge at the upstream.

Table 1. Input data from the source

№	Input data	Data source	Overview
1	Precipitation data (monthly: 2000, 2010, 2020)	Funk et al. (2015)	CHIRPS data is a 35+ year quasi-global rainfall data set. Spanning 50°S-50°N (and all longitudes) and ranging from 1981 to near-present [17].
2	Evapotranspiration data (monthly: 2000, 2010, 2020)	Running et al. (2019)	MOD16A2GF product is a year-end gap-filled 8-day composite dataset produced at 500 m pixel resolution, and is based on the logic of the Penman-Monteith equation [18].
3	Soil hydrological group data	Ross et al. (2018)	HYSOGs250 m dataset represents a globally consistent, gridded dataset of hydrologic soil groups (HSGs) with a projected resolution of approximately 250 m.
4	Digital elevation model	SRTM (2019)	The 30 m DEM was obtained from the SRTM (2019) database of USGS Earth Explorer.
5	Land use and land cover data (2000, 2010, 2020)	Batnyam et al (2022)	A SVM-based classified land use map of the watershed was obtained from Batnyam et al (2022) [13].
6	Watershed and sub -watershed	Bayanjargal et al (2022)	Delineation of the watershed and its sub-watersheds was created from ArcGIS Hydrology tools based on 30 m resolution SRTM, which were obtained from Bayanjargal et al (2022) [13].
7	Biophysical table	Feldman et al (2000) Allen et al (1998)	CN values for each land use type were obtained from the Hydrologic Modeling System HEC-HMS: technical reference manual [19]. Kc coefficients for each month for each land use type were assigned based on the FAO guideline [20].

The methodology followed a structured workflow, including input data processing, model calibration, and validation (Figure 2). The model was validated using observed data from the monitoring station, comparing predicted and observed monthly averages. Model performance was assessed using statistical indicators, including the Nash-Sutcliffe Efficiency (NSE), percentage bias (PBIAS), and the coefficient of determination (R^2). The classification framework proposed by Rauf and Ghumman [16] was applied for result interpretation.

The InVEST SWY model requires input data including monthly average precipitation, evapotranspiration data, a digital elevation model (DEM), land use/land cover (LULC), soil hydrological group, and a biophysical table containing crop coefficient (K_c values) and curve numbers (CN) by land use and soil type, along with rainfall events and the α, β, and γ parameters. These inputs were obtained from various sources and are summarized in Table 1.

Due to the limited availability of streamflow data in the study area, model calibration was restricted to a single station. To enhance the robustness of model evaluation, a 5-fold cross-validation was conducted using the monthly observed streamflow data from the Baidrag-Baidrag gauging station for the years 2000–2020. This approach involved splitting the data into five subsets, using four for training and one for testing in each iteration. Nonetheless, all key model parameters, including the Curve Number (CN) and crop coefficient (Kc), were assigned based on published literature, global datasets, and regionally adapted sources where available. The parameter values used in this study are consistent with those applied in previous research conducted in semi-arid and Central Asian contexts. The complete biophysical table is provided in Appendix Table 1 in the Supplementary Information. The following section details the model results and their evaluation.

3. RESULT AND DISCUSSION

3.1. Annual changes in water yield components

Over the past two decades, annual precipitation in the Baidrag River Basin increased, ranging from 180.9 to 253.7 mm. Seasonal analysis shows fluctuations during the warm season, with 137.4 mm in 2000, rising to 235.9 mm in 2010, and decreasing to 183.0 mm in 2020. Higher precipitation was consistently recorded in the northern areas, near the Khangai Mountains (Figure 3).

To address the potential bias in satellite precipitation data, CHIRPS monthly values were compared with measured precipitation at the Baidrag station from 2000 to 2020. The linear regression showed a strong correlation ($R^2 = 0.79$, $p < 0.001$), indicating that CHIRPS data reliably represent observed precipitation in the basin (Figure 4).

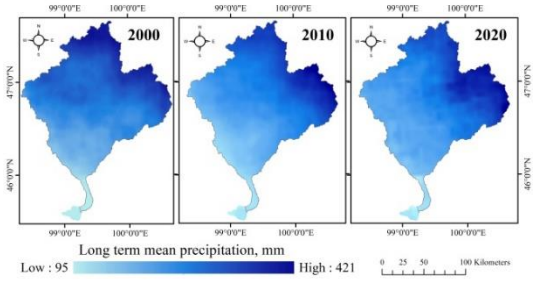

Figure 3. Changes in annual total

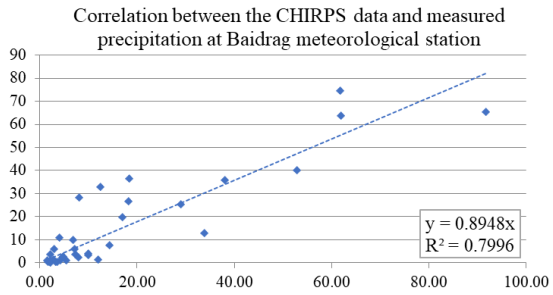

Figure 4. The correlation between the CHIRPS data and the measured precipitation at Baidrag station

Potential evapotranspiration (PET), which reflects atmospheric moisture demand, exhibited a latitudinal gradient that was higher in the southern lowlands and lower in the elevated northern areas (Figure 5). PET decreased from 1314.9 mm in 2000 to 1139.6 mm in 2020, suggesting climatic shifts or land surface changes, particularly in the southern basin. Data gaps in MODIS-based PET outputs were primarily located over Buuntsagaan Lake and sparsely vegetated areas, indicating limitations in remote sensing accuracy under arid and heterogeneous land cover conditions.

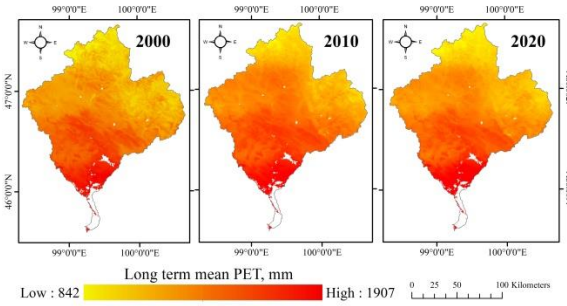

Figure 5. Changes in annual total PET

The spatial distribution of actual evapotranspiration (AET), modeled using InVEST-SWYM, showed clear temporal and spatial variability (Figure 6). In 2000, AET averaged 163.4 mm, with higher values in the north. By 2010, the mean AET slightly declined to 157.99 mm, likely due to drier conditions or reduced vegetation. In 2020, AET increased significantly to 230.14 mm, indicating enhanced soil moisture availability or land cover changes. Comparative analysis of PET and AET further highlights the gap between atmospheric demand and actual water loss. In 2000 and 2010, AET was substantially lower than PET (163.4 mm vs. 1314.9 mm and 157.99 mm vs. 1155.7 mm, respectively). In 2020, despite a slight decrease in PET, AET rose markedly to 230.14 mm, suggesting improved moisture retention or increased vegetation cover.

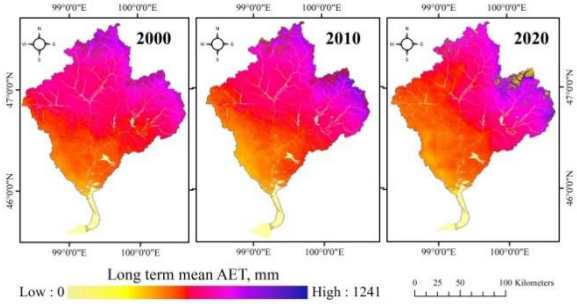

Figure 6. Changes in annual total AET

Annual quickflow (QF), representing surface runoff, showed a rising trend from 2000 to 2020 (Figure 7). In 2000, QF was low (mean: 15.15 mm), reflecting limited runoff. By 2010, QF increased sharply (mean: 24.87 mm), possibly due to intensified rainfall or reduced infiltration capacity. In 2020, QF remained elevated (mean: 21.77 mm), indicating continued hydrological responsiveness to precipitation events.

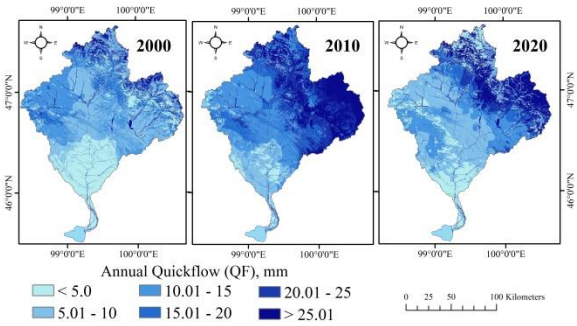

Figure 7. Changes in annual quickflow (QF)

Baseflow (BF) values remained consistently low across the basin (Figure 8), with most areas showing 0.1–4 mm in 2000 and 2010. Slightly higher baseflow (up to 6–8 mm) occurred in localized northern and northeastern zones, reflecting topographic and soil influences. These patterns suggest minimal groundwater contribution, with slightly higher baseflow in the northern uplands due to better infiltration conditions.

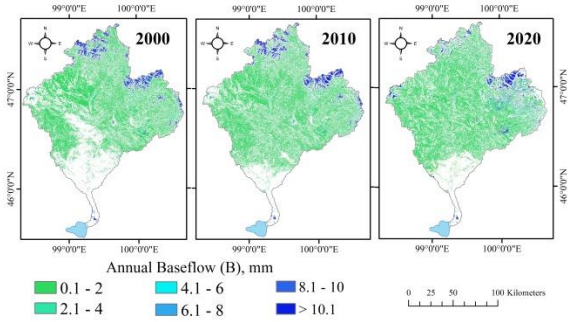

Figure 8. Changes in annual base flow (BF)

3.2. Seasonal changes in Quickflow estimation

Figure 9-11 illustrates the spatial and temporal distribution of quickflow (QF) for 2000, 2010, and 2020. Across all years, QF exhibited clear seasonality, with peak values occurring during summer (June–August), particularly in July (2000, 2020) and June (2010). Mean peak QF values were 5.07 mm in 2000, 10.68 mm in 2010, and 10.73 mm in 2020, predominantly in the northern and western sub-basins, where increased precipitation and terrain steepness enhanced surface runoff.

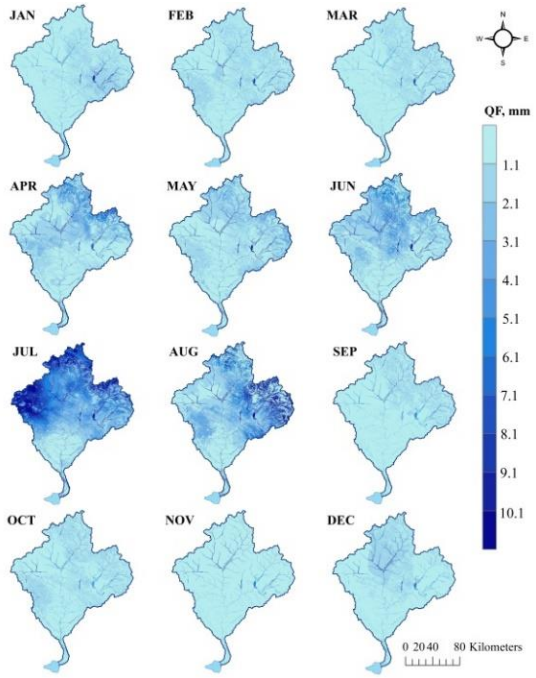

Figure 9. Monthly maps of quickflow, 2000

QF during winter (October–April) remained low across all years, with mean values below 1.72 mm in 2000, 2.72 mm in 2010, and 0.94 mm in 2020, reflecting limited runoff due to low temperatures and ground freezing. Transitional months (May, September) showed moderate increases or declines, marking the start or end of the runoff season. These patterns emphasize the influence of seasonal precipitation, topography, and land cover on QF dynamics.

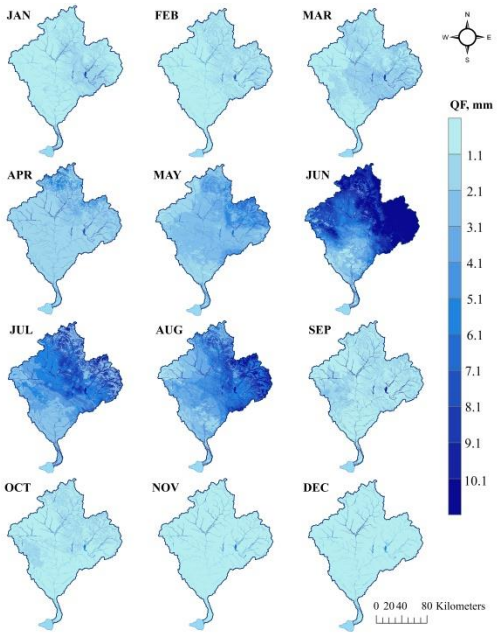

Figure 10. Monthly maps of quickflow, 2010

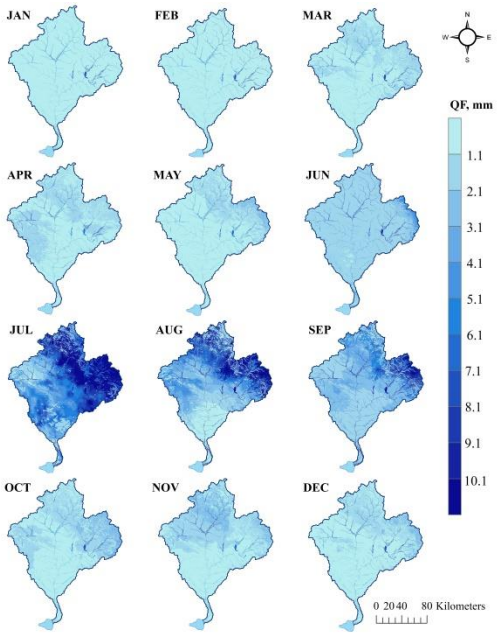

Figure 11. Monthly maps of quickflow, 2020

In 2000, spring QF ranged from 1.43–2.54 mm (9.66–17.73 m^3/s), summer peaked at 5.07 mm (34.25 m^3/s) in July, while autumn and winter values dropped below 0.4 mm (Figure 9). In 2010, spring QF increased notably (2.72–10.68 mm; 18.78–74.54 m^3/s), with a peak in June, while other seasons followed the same

low-flow pattern (Figure 10). By 2020, spring flows declined (0.56–0.85 mm), but summer QF again peaked in July at 10.73 mm (72.48 m^3/s), aligning with the year's highest precipitation (91.71 mm) (Figure 11).

The findings reveal strong interannual and seasonal variability in QF, closely tied to precipitation intensity and distribution, with higher runoff in the northern and western regions indicating the combined effects of climate, elevation, and land characteristics on surface hydrology.

3.3. Validation of seasonal quickflow estimation

Model validation was performed by comparing simulated quickflow with observed monthly streamflow data from the Baidrag-Baidrag gauging station for the years 2000 and 2020.

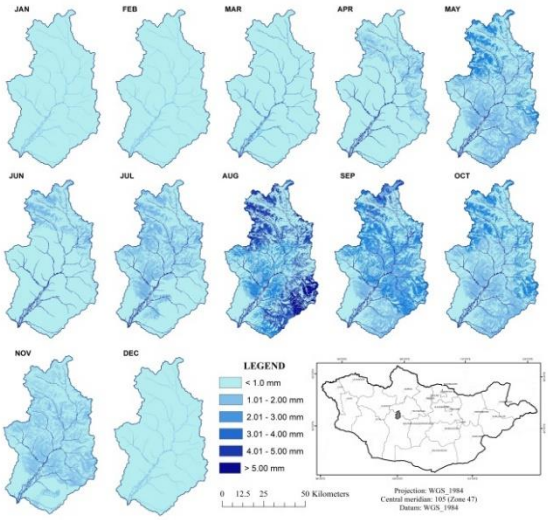

Figure 12. Estimated QF for sub-basin, 2000

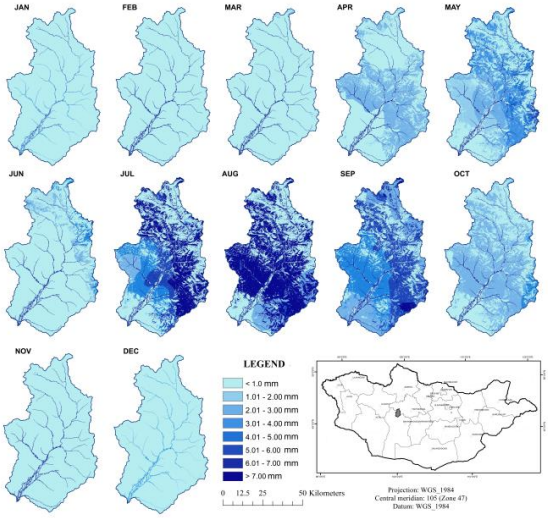

Figure 13. Estimated QF for sub-basin, 2020

Although several hydrological stations exist in the Baidrag River-Buuntsagaan Lake Basin (e.g., Zag-Zag, Tsagaanturuut-Galuut, Baidrag-Baidrag, and Baidrag-Bayanburd), limited spatial coverage restricted validation to a single station. The monitoring density in the basin, approximately one station per 7,100 km^2, is significantly below global standards, limiting comprehensive calibration efforts. Thus, we selected the model result at the sub-basin level for validating only against the Baidrag-Baidrag station (area ~ 3360.7 km^2) as shown in Figure 12, Figure 13.

As observed from the Figure 14, the model tended to overestimate streamflow during the spring snowmelt (May) and underestimate it during the summer rainfall season. These deviations are likely attributed to the CHIRPS precipitation data used as input. In future studies, incorporating ground-based precipitation measurements and calculating evapotranspiration based on observed climate variables such as air temperature, relative humidity, and solar radiation may help to reduce this difference and improve the accuracy of model outputs.

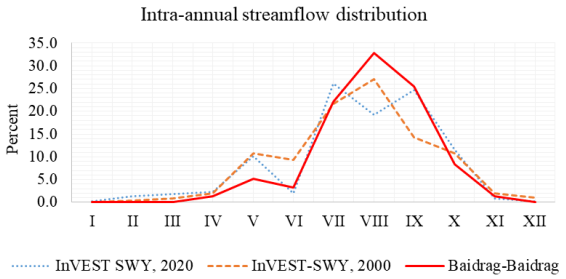

Figure 14. Intra-annual streamflow distribution (Observed Data and Model Results)

Model performance was assessed using Nash–Sutcliffe Efficiency (NSE) and Percent Bias (PBIAS), following the criteria by Moriasi et al. [21] as depicted in Figure 15. NSE values of 0.77 (2000) and 0.79 (2020) indicate "very good" performance, while PBIAS values of 25.64 (2000) and –23.64 (2020) reflect "satisfactory" performance. The coefficient of determination (R^2=0.81) further supports a "strong correlation" between observed and predicted streamflow values.

While validation using annual data for 2000 and 2020 indicated strong model performance, further evaluation was necessary to assess the model's robustness across varying temporal conditions. To this end, a 5-fold cross-validation was conducted using monthly observed and simulated streamflow data from the Baidrag station for the period 2000–2020. The resulting NSE values were 0.477, 0.332, 0.610, 0.890,

and 0.871, with an average NSE of 0.636. These results indicate "moderate to good" agreement between observed and simulated flows and support the temporal robustness and generalizability of the model, despite the scarcity of in-situ hydrological data.

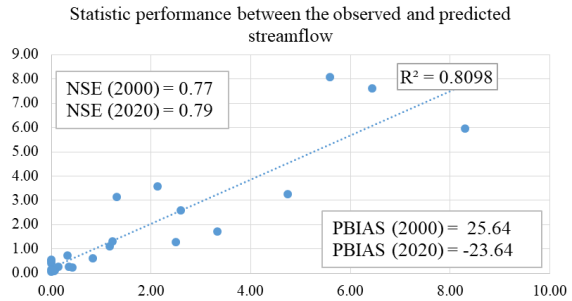

Figure 15. The correlation between the observed and simulated streamflow (R^2, NSE, PBIAS)

The reliance on a single gauging station for model validation represents a key limitation, as it restricts spatial assessment of model performance across the wider basin. While the 5-fold cross-validation provided additional insight into temporal robustness, the generalizability of the model's outputs to ungauged sub-basins remains uncertain. Future studies should prioritize the expansion of monitoring infrastructure and explore the integration of remote sensing products or regional flow estimates to support broader validation efforts in data-scarce regions.

4. CONCLUSION

This study applied the InVEST Seasonal Water Yield Model to assess hydrological dynamics in the Baidrag River Basin from 2000 to 2020. The findings reveal marked spatial and seasonal variability in water yield, demonstrating the model's utility in semi-arid, data-scarce regions. Annual precipitation fluctuated substantially, increasing from 180.9 mm in 2000 to 253.7 mm in 2010, then declining to 183.0 mm in 2020. Quickflow (QF) mirrored this trend, with modeled means of 15.15 mm, 24.87 mm, and 21.77 mm, respectively. Peak QF occurred in summer, particularly July, except in 2010 when the maximum shifted to June. Winter QF remained consistently low (<2 mm), indicating suppressed runoff due to cold conditions and possible ground freezing.

Actual evapotranspiration (AET) rose from 163.4 mm to 230.14 mm over the study period, despite a decline in potential evapotranspiration (PET), suggesting increased soil moisture or vegetation response. Baseflow remained low throughout the study period, with values generally under 8 mm across the basin, underscoring the dominant role of quickflow and limited subsurface contribution to total runoff.

Model validation against observed streamflow at the Baidrag-Baidrag station indicated "very good" NSE values, although some seasonal bias was noted, such as overestimation in spring and underestimation in summer, likely due to CHIRPS data limitations and the absence of snowmelt representation.

Overall, the InVEST-SWYM model effectively captured seasonal water yield patterns and runoff dynamics in the Baidrag River Basin, demonstrating its applicability in data-scarce, semi-arid environments. The results provide valuable insights to support water resource management and land-use planning. However, several limitations should be addressed in future research. The absence of a snowmelt component likely contributes to the underestimation of spring streamflow, particularly in high-elevation zones. Similarly, reliance on CHIRPS precipitation data—though generally reliable—may introduce uncertainty during transitional seasons due to its limited ability to capture localized events. The scarcity of hydrological gauge stations further constrains the validation of spatial runoff estimates. To improve model accuracy, future efforts should incorporate snowmelt routines, enhance precipitation inputs through blended satellite and ground-based datasets, and expand the hydrological monitoring network.

Additionally, given the constraints of input data and computational scope, this study did not include formal sensitivity or uncertainty analyses. However, future applications of the InVEST-SWYM model in similar data-scarce basins should consider incorporating parameter sensitivity testing and probabilistic uncertainty assessments (e.g., Monte Carlo methods) to enhance understanding of model robustness and improve confidence in simulation outputs.

ACKNOWLEDGEMENTS

This research was conducted under the framework of the UNDP-ENSURE project titled "Assessing the ecological capacity of the Baidrag River Basin at the landscape level for further action to protect and use it properly" (No. c_Prof/2022/019). We are gratefully thankful to the support of the project leader Ph.D S.Narangerel and researchers of the division of Physical Geography (IGG, MAS). Special thanks are extended to Ms. Duuren, expert at the Buuntsagaan-Orog Lake Basin Authority, for her valuable assistance.

REFERENCES

[1] B. Burkhard, F. Kroll, S. Nedkov, and F. Müller, "Mapping ecosystem service supply, demand and budgets," *Ecological indicators*, vol. 21, pp. 17–29, 2012. Available: doi: 10.1016/j.ecolind.2011.06.019.

[2] R. O. TEEB, "Mainstreaming the Economics of Nature," 2010. ISBN: 978-3-9813410-0-4.

[3] NRCS (Natural Resources Conservation Service), "National engineering handbook," 2009.

[4] S. Halder, S. Das, and S. Basu, "Estimation of seasonal water yield using InVEST model: a case study from West Bengal, India," *Arabian Journal of Geosciences*, vol. 15, no. 14, pp. 1–18, 2022. Available: doi: 10.1007/s12517-022-10551-2.

[5] H. Lu *et al.*, "Spatiotemporal Water Yield Variations and Influencing Factors in the Lhasa River Basin, Tibetan Plateau," *Water*, vol. 12, no. 5, 2020. Available: doi: 10.3390/w12051498.

[6] J. Vila-Traver, E. Aguilera, J. Infante-Amate, and M. González de Molina, "Climate change and industrialization as the main drivers of Spanish agriculture water stress," *Science of The Total Environment*, vol. 760, pp. 143399, Mar. 2021. Available: doi: 10.1016/j.scitotenv.2020.143399.

[7] D. Molden, T. Oweis, P. Steduto, P. Bindraban, M. A. Hanjra, and J. Kijne, "Improving agricultural water productivity: Between optimism and caution," *Agricultural Water Management*, vol. 97, no. 4, pp. 528–535, Apr. 2010. Available: doi: 10.1016/j.agwat.2009.03.023.

[8] D. dos R. Pereira, M. A. Martinez, F. F. Pruski, and D. D. da Silva, "Hydrological simulation in a basin of typical tropical climate and soil using the SWAT model part I: Calibration and validation tests," *Journal of Hydrology: Regional Studies*, vol. 7, pp. 14–37, Sep. 2016. Available: doi: 10.1016/j.ejrh.2016.05.002.

[9] J. Norvanchig and T. O. Randhir, "Simulation of ecohydrological processes influencing water supplies in the Tuul River watershed of Mongolia," *Journal of Hydroinformatics*, vol. 23, no. 5, pp. 1130–1145, 2021. Available: doi: 10.2166/hydro.2021.056

[10] B. Dorjsuren *et al.*, "Study on relationship of land cover changes and ecohydrological processes of the Tuul River Basin," *Sustainability*, vol. 13, no. 3, pp. 1153, 2021. Available: doi: 10.3390/su13031153.

[11] C. Sukhbaatar, R. U. Sajjad, J. Lunten, S. Yu, and C. Lee, "Climate change impact on the Tuul river flow in a Semiarid region in Mongolia," *Water Environment Research*, vol. 89, no. 6, pp. 527–538, 2017. Available: doi: 10.2175/106143016X14798353399223.

[12] J. W. Redhead *et al.*, "Empirical validation of the InVEST water yield ecosystem service model at a national scale," *Science of the Total Environment*, vol. 569, pp. 1418–1426, 2016. Available: doi: 10.1016/j.scitotenv.2016.06.227.

[13] Institute of Geography and Geoecology, "Assessment of the Ecological capacity of the Baidrag river basin at the landscape level for further action to protect and use it properly," Ulaanbaatar, UNDP-Consulting Service, 2022.

[14] G. Davaa, Ed., *Surface water regime and resources of Mongolia*. 2015.

[15] R. Sharp *et al.*, "InVEST 3.7. 0 user guide. Collaborative publication by The Natural Capital Project," 2019.

[16] A. Rauf and A. R. Ghumman, "Impact assessment of rainfall-runoff simulations on the flow duration curve of the Upper Indus River—A comparison of data-driven and hydrologic models," *Water*, vol. 10, no. 7, pp. 876, 2018. Available: doi: 10.3390/w10070876.

[17] C. Funk, A. Verdin, J. Michaelsen, P. Peterson, D. Pedreros, and G. Husak, "A global satellite-assisted precipitation climatology," *Earth System Science Data*, vol. 7, no. 2, pp. 275, 2015. Available: doi: 10.5194/essd-7-275-2015.

[18] S. Running, Q. Mu, M. Zhao, and A. Moreno, "MOD16A2GF MODIS/Terra Net Evapotranspiration Gap-Filled 8-Day L4 Global 500 m SIN Grid V006," *NASA EOSDIS Land Processes DAAC*, 2019.

[19] A. D. Feldman, *Hydrologic modeling system HEC-HMS: technical reference manual*. US Army Corps of Engineers, Hydrologic Engineering Center, 2000.

[20] R. G. Allen, L. S. Pereira, D. Raes, and M. Smith, "Crop evapotranspiration-Guidelines for computing crop water requirements-FAO

Irrigation and drainage paper 56," *Fao, Rome*, vol. 300, no. 9, p. D05109, 1998, ISBN: 92-5-104219-5.

[21] D. N. Moriasi, J. G. Arnold, M. W. Van Liew, R. L. Bingner, R. D. Harmel, and T. L. Veith, "Model evaluation guidelines for systematic quantification of accuracy in watershed simulations," *Transactions of the ASABE*, vol. 50, no. 3, pp. 885–900, 2007. Available: doi: 10.13031/2013.23153.

5. SUPPLEMENTARY INFORMATION

Appendix Table 1: Biophysical Table Containing Model Parameters

(Land use/land cover (LULC) classes with assigned monthly crop coefficients (Kc) and Curve Numbers (CN) for four hydrological soil groups (A–D). The watershed-level baseflow model parameters used in the InVEST-SWYM model were $\alpha = 0.08$, $\beta = 1.0$, and $\gamma = 1.0$, as recommended in the model documentation)

LULC name	Kc_1	Kc_2	Kc_3	Kc_4	Kc_5	Kc_6	Kc_7	Kc_8	Kc_9	Kc_10	Kc_11	Kc_12	CN_A	CN_B	CN_C	CN_D
Forest	0	1	1	1	1	1	1	1	1	1	1	1	36	60	73	79
Meadow	0.05	0.05	0.2	0.3	0.4	0.8	0.9	0.8	0.4	0.3	0.1	0.05	30	58	71	78
Saline meadow	0.03	0.03	0.1	0.1	0.1	0.3	0.3	0.3	0.7	0.7	0.7	0.05	49	68	79	84
Mountain meadow	0.03	0.5	0.8	0.8	0.8	1	1	1	0.95	0.95	0.95	0.2	35	56	70	77
Dry steppe	0.05	0.1	0.3	0.3	0.3	1.15	1.15	1.15	1.1	1.1	1.1	0.4	68	79	86	89
Desert steppe	0.1	0.15	0.4	0.4	0.4	0.6	0.6	0.6	0.5	0.5	0.5	0.3	55	72	81	86
Semi steppe	0.05	0.05	0.2	0.2	0.2	0.3	0.3	0.3	0.25	0.25	0.25	0.1	63	77	85	88
Settlement	0.01	0.01	0.12	0.12	0.12	0.32	0.32	0.32	0.22	0.22	0.22	0.1	72	82	87	89
Agriculture land	0.05	0.05	0.2	0.4	0.8	1	1.05	1	0.8	0.3	0.2	0.2	49	69	79	84
Water bodies	0.055	0.055	0.25	0.25	0.25	0.65	0.65	0.65	1.25	1.25	1.25	1	99	99	99	99
High mountain tundra	0.02	0.02	0.15	0.15	0.15	0.2	0.2	0.2	0.05	0.05	0.05	0.02	63	77	85	88

Appendix Table 2: Summary of estimated seasonal quickflow and precipitation results with observed data (2000, 2010, and 2020)

(Seasonal precipitation and quickflow (QF) estimates from the InVEST-SWYM model for the years 2000, 2010, and 2020, including simulated quickflow in millimeters and cubic meters per second (cumecs), CHIRPS-derived precipitation inputs, and observed precipitation data from the Baidrag station)

2000	InVEST SWY result		Precipitation		**2010**	InVEST SWY result		Precipitation		**2020**	InVEST SWY result		Precipitation	
	QF (mm)	QF (cumecs)	CHIRPS	Observed		QF (mm)	QF (cumecs)	CHIRPS	Observed		QF (mm)	QF (cumecs)	CHIRPS	Observed
Jan	0.09	0.61	1.69	0.30	Jan	0.11	0.74	2.15	3.6	Jan	0.1	0.68	2.83	1.3
Feb	0.08	0.60	1.49	1.10	Feb	0.18	1.35	2.13	0.9	Feb	0.24	1.79	4.67	2.4
Mar	0.15	1.01	2.93	5.90	Mar	0.32	2.16	4.82	2.6	Mar	0.31	2.09	7.89	2.4
Apr	1.72	12.01	5.49	0.90	Apr	2.72	18.98	6.77	9.9	Apr	0.63	4.40	9.97	4.1
May	1.43	9.66	10.00	3.40	May	2.78	18.78	18.36	36.5	May	0.85	5.74	14.26	7.7
Jun	2.54	17.73	28.97	25.30	Jun	10.68	74.54	61.80	74.7	Jun	0.56	3.91	16.90	19.9
Jul	5.07	34.25	61.95	40.10	Jul	5.12	34.58	38.03	35.8	Jul	10.73	72.48	91.71	65.6
Aug	2.93	19.79	52.83	63.70	Aug	1.09	7.36	33.79	12.8	Aug	5.91	39.92	67.73	*
Sep	0.47	3.28	8.05	28.40	Sep	1.37	9.56	12.42	32.8	Sep	1.08	7.54	18.27	26.8
Oct	0.4	2.70	7.31	3.60	Oct	0.35	2.36	7.10	6.1	Oct	0.94	6.35	11.96	1.3
Nov	0.13	0.91	4.15	1.00	Nov	0.1	0.70	3.15	0.3	Nov	0.26	1.81	4.01	10.8
Dec	0.14	0.95	3.53	0.40	Dec	0.06	0.41	2.06	0.6	Dec	0.16	1.08	2.15	0